Biophysical Chemistry 141 (2009) 153–161

Contents lists available at ScienceDirect

Biophysical Chemistry

journal homepage: http://www.elsevier.com/locate/biophyschem

Behaviour of a peptide sequence from the GB virus C/hepatitis G virus E2 protein in Langmuir monolayers: Its interaction with phospholipid membrane models

Silvia Pérez-López [a,b], Marina Nieto-Suárez [a], Concepció Mestres [b], M. Asunción Alsina [b], Isabel Haro [c], Nuria Vila-Romeu [a,*]

[a] Department of Physical Chemistry, Faculty of Sciences, University of Vigo, Campus Universitario As Lagoas s/n 32004 Ourense, Spain
[b] Department of Physical Chemistry, Faculty of Pharmacy, University of Barcelona, Av. Joan XXIII s/n 08028 Barcelona, Spain
[c] Unit of Synthesis and Biomedical Application of Peptides, Department of Biomedical Chemistry, IQAC-CSIC Barcelona, Spain

ARTICLE INFO

Article history:
Received 22 December 2008
Received in revised form 21 January 2009
Accepted 22 January 2009
Available online 30 January 2009

Keywords:
Hepatitis G
GBV-C/HGV
Membranes
Fusion peptide
Phospholipid Langmuir monolayers
BAM

ABSTRACT

The GB virus C/hepatitis G virus (GBV C/HGV) is a Flaviviridae member that despite its non pathogenicity, has become of great interest given that it could inhibit the replication of the human immunodeficiency virus (HIV). Therefore, a better knowledge of the virus peptides involved in the cellular membrane fusion mechanism has become our aim. The selected peptide, named E2(347–363), corresponds to the GBV-C/HGV E2 protein and has been synthesized in order to study its interaction with *in vitro* membrane models. Two phospholipids, varying the charge and the unsaturations of the hydrocarbon chain have been chosen: 1,2-dipalmitoyl-sn-glycero-3-phosphocholine (DPPC) and 1,2-dioleoyl-sn-glycero-3-[phospho-rac-(1-glycerol)] (sodium salt) (DOPG). For our porpoise, we have used the Langmuir monolayer technique and Brewster angle microscopy (BAM) to gain deeper insight into the peptide/lipid interactions. The results obtained allow us to argue in favour of considering E2(347–363) a success candidate for developing further experiments in order to determine its potential role in the GBV C/HGV virus/cell membrane fusion process.

1. Introduction

The GB virus C (GBV-C) and the hepatitis G virus (HGV) are strain variants of an enveloped RNA *Flaviviridae* member virus, which was simultaneously discovered in 1996 by two different research teams [1,2]. This enveloped RNA *Flaviviridae* member virus has been referred to as both, GBV-C and HGV, with its current taxonomic name being GBV-C/HGV. Infection with GBV-C/HGV is relatively common and has been found worldwide. It is known that between 1% and 4% of healthy blood donors have had GBV-C/HGV RNA in their sera [3–5]. Although GBV-C/HGV has not been associated with any particular disease despite numerous researches [6,7], some reports have shown GBV-C/HGV to have a profound "protective" influence on the human immunodeficiency virus (HIV) in the situation of co-infection [8]. This co-infection is particularly high with GBV-C/HGV; several studies have suggested that it varies between 14% and 45%, with higher rates occurring in homosexual men and intravenous drug users [9–11]. Although recent research has identified a number of putative pathways, the mechanism involved in the beneficial effect of GBV-C/HGV on the course of HIV infection remains obscure.

These enveloped viruses, i.e., HIV and GBV-C/HGV, infect host cells by fusing their envelope with the external cellular membrane [12,13]. It is known that in eukaryotes, this process is mediated by viral proteins, which help the virus introduce its genetic material into the host cells [14,15]. The first step in a cell infection consists in the binding of certain proteins with specific receptors on the membrane, which can be either proteins, lipids or carbohydrates. This binding plays an essential role in cell infection because it induces conformational changes in the viral protein, resulting in the exposure of its hydrophobic peptides, loops or patches (the so-called "fusion peptides") [16,17], which are responsible for the virus's entry into the cell. However, the nature of the interaction of these viral fusion proteins with membranes and the mechanism by which these proteins accelerate the formation of membrane fusion intermediates are still unknown.

It has been described in the literature that one of these proteins, the GBV-C/HGV E2 protein, regulates the entrance of HIV into the cell [18]. The two structural envelope glycoproteins, E1 and E2 of GBV-C/HGV, are located within the amine-terminus of the polyprotein, while the nonstructural proteins reside within the carboxy-terminal part (Fig. 1) [19]. Furthermore, the E2 protein of other *Flaviviridae* member, i.e., the hepatitis C virus (HCV), is also involved in the process of cell infection [20]. It is known that, for the hepatitis C E2 protein, there is a fragment near the carboxy-terminus called a fusion peptide that belongs to the class II internal fusion peptides described for other viruses [21]. Thus, the identification of the GBV-/HGV E2 fusion

* Corresponding author. Faculty of Sciences, University of Vigo, Campus Universitario As Lagoas s/n 32004, Ourense, Spain. Tel.: +34 988387095; fax: +34 988387001.
E-mail address: nvromeu@uvigo.es (N. Vila-Romeu).

0301-4622/$ – see front matter © 2009 Elsevier B.V. All rights reserved.
doi:10.1016/j.bpc.2009.01.007

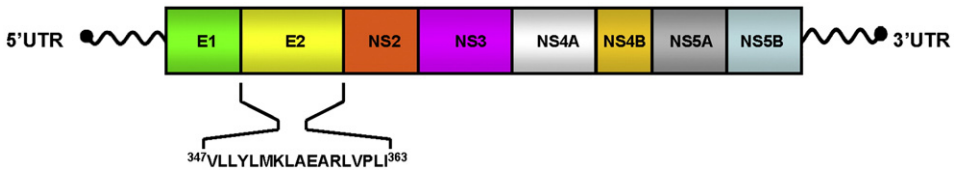

Fig. 1. Genomic organization of the GBV-C/HGV genome showing 5′ and 3′ un-translated regions (UTR). The genome is composed of single stranded, positive sense RNA (ss + RNA). The synthesized peptide ^{347}VLLYLMKLAEARLVPLI^{363} is marked in the figure. Genes are not shown to scale.

peptide could shed light on the mechanism by which GBV-C/HGV infects cells and inhibits the replication of HIV. To achieve this purpose, we have compared different strains of the protein E2 (from GBV-C/HGV virus) obtained from the Gene Data Bank. With the aim of selecting a conserved region, different geographical strains were compared (Africa, Japan, North America, and Europe). Furthermore, we applied different theoretical algorithms to select the peptide corresponding to the well-preserved sequence 347–363 (NH_2–VLLYLMKLAEARLVPLI–$CONH_2$).

Understanding the interactions between the viral fusion peptides and the cell membrane seems to be crucial in order to elucidate the viral entry mechanism into cells. These peptide–membrane interactions have been studied using different biophysical techniques, where lipidic vesicles were mainly used to mimic biological membranes [22]. Organized lipid layers of molecular dimensions, which are spread at the air–water interface, have been widely used as a simplified approach to developing *in vitro* membrane models. These layers, named Langmuir monolayers [23], are a traditional but powerful system that has provided the best understanding of the behaviour of amphiphilic molecules at the air–water interface, and Langmuir monolayers also enable us to study intermolecular interactions in a two-dimensional (2D) multi-component system. Using this technique, we can control the monolayer composition, the surface pressure, and the molecular orientation at the interface. Many authors have used these *in vitro* models to study the interactions between different peptides or proteins and membranes [24–26].

As it is known, the lipid fraction of biological membranes is mainly composed of phospholipids, with varying chain length and ionic character [27]. With the aim of building an *in vitro* membrane model, we have selected two lipids with differing head group net charge and differing degree of unsaturation in their hydrocarbon chains: 1,2-dipalmitoyl-*sn*-glycero-3-phosphocholine (DPPC), a major component of biological membranes [28], and 1,2-dioleoyl-*sn*-glycero-3-[phospho-*rac*-(1-glycerol)] (sodium salt) (DOPG) an anionic, fluid lipid. In order to determine the ability of these lipid monolayers to host the selected peptide sequence, we have studied the behaviour of pure and mixed peptide–lipid monolayers spread at the air–water interface, by analyzing and recording the surface pressure (π) – mean molecular area (A) isotherms. Furthermore, Brewster angle microscopy (BAM), which is extensively used in studying the interactions between peptides and lipids at the interface [29,30], has provided complementary information about the morphology of the monolayers.

2. Materials and methods

2.1. Lipids and chemicals

1,2-dipalmitoyl-*sn*-glycero-3-phosphocholine and 1,2-dioleoyl-*sn*-glycero-3-[phospho-*rac*-(1-glycerol)] (sodium salt) were purchased from Avanti Lipids. Spreading solutions were prepared in a mixture of chloroform and methanol (9:1:v/v) both proanalysis and purchased from Merck (Poole, Dorset, U.K.). The aqueous subphase was 4-(2-hydroxyethyl)-1-piperazineethanesulfonic acid (HEPES) 5 mM, NaCl 100 mM pH 7.4 (Sigma-Aldrich); it was prepared with ultrapure water produced by deionization and Nanopure purification coupled to a Milli-Q purification system (Milli-Q system, Millipore Corp.) up to a resistivity of 18.2 MΩ cm.

N-α-Fluorenylmethoxycarbonylamino acids and Rink amide resin were obtained from Novabiochem (Nottingham, U.K.). Dimethylformamide (DMF), dichloromethane (DCM), acetonitrile and 20% piperidine/DMF were purchased from Fluka. Washing solvents such as acetic acid and diethyl ether, were obtained from Merck (Poole, Dorset, U.K.). Trifluoroacetic acid (TFA) was supplied by Fluka (Buchs, Switzerland). *N*-hydroxybenzotriazole (HOBt), *N,N*′-diisopropylcarbodiimide (DIPCDI), and 2-(1*H*-benzotriazole-1-yl)-1-3-3-tetramethyluroniumtetrafluoroborate (TBTU) coupling reagents were obtained from Novabiochem. *N,N*-diisopropylethylamine (DEIA) was obtained from Merck. 1,8-diazabicyclo [5.4.0]undec-7-ene and 1,2-ethanedithiol (EDT) were purchased from Aldrich.

2.2. Peptide synthesis

The synthesis was carried out on a Rink amide resin, with a functionalization of 0.479 mEq g^{-1}. Briefly, a 9-fluoromethylmethoxy carbonyl/*tert*-butyl (Fmoc/tBu) strategy by means of DIPCDI/HOBt activation and TBTU and DEIA reagents for difficult couplings were used. Side protection was effected by the following: 2,2,5,7,8-pentamethylchroman-6-sulfonyl (Pmc) for Arg, tBu for Tyr, and *tert*-butoxycarbonyl (Boc) for Lys. Threefold molar excess of Fmoc amino acids was used throughout the synthesis. The stepwise addition of each residue was assessed by Kaiser's (ninhydrin) test. Deprotection was performed in 20% piperidine/DMF. We have used 1,8-diazabicyclo [5.4.0]undec-7-ene for difficult deprotections. To cleave the peptide from the resin and to remove the side chain blocking groups, the resin was treated with trifluoroacetic acid (TFA) solution containing appropriate scavengers such as TFA:H_2O:EDT in a ratio of 95:2.5:2.5.

2.3. Methods

The experiments were carried out on the KSV LB3000 Langmuir trough (KSV, Finland), total area = 0.087 m^2 (0.58 m · 0.15 m), equipped with two symmetrical mobile barriers. All of the investigated film-forming molecules were dissolved in a chloroform/methanol (9:1:v/v) mixture at concentrations of 0.3–0.5 mg mL^{-1}. The stock solutions were mixed in appropriate proportions and dropped, using a Hamilton microsyringe, onto the surface of HEPES 5 mM, NaCl 100 mM, pH 7.4. Twenty minutes were allowed for the evaporation of the spreading solvent, after which the monolayers were compressed with a speed of 0.02 m min^{-1}. The surface pressure was monitored continuously by an electronic microbalance with an accuracy of ±0.05 mN m^{-1}, using a platinum plate as the pressure sensor. The Langmuir trough was thermostated with a Julabo® circulating water bath with an accuracy of ±1.5 K. The experiments were carried out at 293 K. All of the presented π–A isotherms have been selected after being reproduced in at least three independent experiments.

A Brewster Angle Microscope BAM2*plus* (NFT, Germany) was used for the microscopic observation of the monolayer morphology. It was equipped with a 50 mW laser, emitting *p*-polarized light (532 nm wavelength) that was reflected off the air–water interface at approximately 53.15° (Brewster angle). The lateral resolution of the

Table 1
Peptide characterization.

Peptide	Amino acid sequence[a]	Net charge	HPLC (k′)[b]	ES-MS[c]
E2(347–363)	VLLYLM*K*LA*E*A*R*LVPLI	+1	5.25	$M^+ = 1954.21$

High performance liquid chromatography (HPLC) conditions: A: H_2O [0.05% trifluoroacetic acid (TFA)]; B: acetonitrile (0.05% TFA). Gradient 95% *A* to 5% *A* in 30 mm; 1:215 nm, 1 mL min^{-1}. Kromasil C-18 column. Detection: 215 and 280 nm.
[a] In italics and bold the cationic amino acid, in grey and underlined the anionic amino acid.
[b] Capacity factor.
[c] Electrospray mass spectrometry (ES-MS).

microscope was 2 μm. The images were digitized and processed to obtain the best quality BAM pictures.

3. Results and discussion

3.1. Peptide selection and synthesis

The selection of putative antigenic domains of the GBV-C/HGV E2 protein was performed by the alignment of several published sequences of virus isolates. The consensus sequence was obtained by means of a comparative study of the GBV-C/HGV isolates using the Clustalw program [31]. Next, this sequence was studied using the computerized prediction of its antigenicity after analyzing the hydrophilicity [32] and the accessibility profiles of the proteins according to Janin [33], Welling [34], and Chou and Fasman [35]; these characteristics are considered good predictors for defining the antigenic sites within proteins. From these algorithms, a sequence of 17 residues was selected in accordance with the literature about fusion peptides [36]. The synthesis of E2(347–363) was performed and accomplished by an Fmoc-based solid phase methodology, as described in the Peptide synthesis section. Yields based on peptidyl–resin weight increase were almost quantitative. The purity of the samples after high performance liquid chromatography (HPLC) purification was checked by analytical HPLC and was found to be higher than 95% in all cases. The sequence and characterization of the peptide is shown in Table 1. E2(347–363) is a net positively charged peptide; it contains a two positively charged amino acids (Lys353 and Arg358), which could be important for the interaction with negatively charged phospholipid membranes and the negatively charged amino acid (Glu356).

3.2. Mixed monolayers of E2(347–363)/DPPC

The isotherms of pure DPPC and E2(347–363), as well as the E2 (347–363)/DPPC mixtures are shown in Fig. 2A. Monolayers were spread on a HEPES 5 mM, NaCl 100 mM pH 7.4 subphase at 293 K. The pure DPPC underwent a first order phase transition from a liquid-expanded (LE) to a liquid-condensed (LC) phase denoted by a *plateau* in the course of the *π–A* curve at about 5 mN m^{-1} (transition pressure, π_t), and the monolayer collapsed at ~70 mN m^{-1}. On the other hand, the E2(347–363) isotherm is characteristic of peptides with low molecular weight [37]. The mean area occupied by each amino acid residue at the interface (~17 $Å^2$) proves that the peptide adopts a well-extended horizontal configuration in the monolayer; other authors have observed values for different peptides which fell from 8 to 23 $Å^2$ $residue^{-1}$ [38–40]. The peptide isotherm exhibited a collapse pressure (π_c) of about 22 mN m^{-1}, which is attributed to the folding of the hydrophobic part to the air and to the partial immersion of the peptide polar groups in the aqueous subphase. The effects on the mean molecular area upon increasing the amount of peptide in the mixtures has been analyzed by the lift-off area, which is defined as the mean molecular area when the surface pressure has reached 1 mN m^{-1} [41]. The isotherms recorded for mixed monolayers were more expanded than the pure DPPC curve, and they showed the peptide collapse starting at the same surface pressure. The lift-off area increased with the peptide molar fraction, from 142.4 $Å^2$ $molecule^{-1}$ corresponding to $X_{E2(347-363)} = 0.2$ to 185.2 at $X_{E2(347-363)} = 0.8$.; that is to say, the isotherms were shifted to higher areas as the $X_{E2(347-363)}$ increased. The DPPC LE–LC phase transition only appeared for mixtures of $X_{E2(347-363)} \leq 0.6$, and the monolayer collapse pressure (for mixed monolayers) could only be obtained for the $X_{E2(347-363)} = 0.2$ where its value changed with respect to the pure DPPC film.

Fig. 2A includes the plots of compressibility modulus (C_s^{-1}) [42], defined as $-A(d\pi/dA)_T$, as a function of the pressure for the different mixtures. The values of C_s^{-1} are very useful to characterise the state and phase transitions of a monolayer upon compression [43]. For LE films, the compressibility modulus ranges from 12.5 to 100 mN m^{-1}, while for LC films values are between 100 and 250 mN m^{-1}. At low surface pressures (<20 mN m^{-1}) the presence of the peptide produced a slight increase in the C_s^{-1} values, even though the monolayer remained in a LE state. As can be seen, C_s^{-1} reached values nearly consistent with a LC state only for $X_{E2(347-363)} = 0.2$.

The analysis of the collapse pressures of pure and mixed monolayers can be helpful in providing insight into the behaviour of these binary systems. Thus, the variation of the monolayer collapse pressure with the composition indicates 2D miscibility of both molecules at the air–water interface [44]. However, we can only prove this for monolayers of $X_{E2(347-363)} = 0.2$. On the other hand, other surface pressure values that require consideration are the collapse pressure of the E2(347–363) (π_c) monolayer and the transition pressure of the DPPC (π_t) film. Both of these are of interest in order to discuss the miscibility of the components in the monolayer. In all the mixtures, the peptide collapsed at the same surface pressure

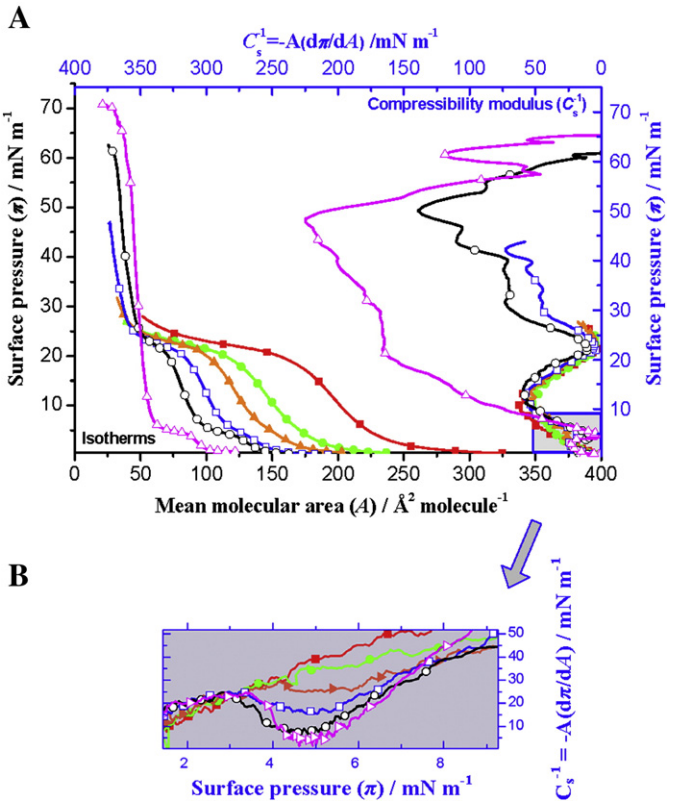

Fig. 2. (A) Surface pressure (π)–mean molecular area (A) isotherms of pure and mixed E2(347–363)/DPPC monolayers spread on subphase HEPES 5 mM, NaCl 100 mM pH 7.4 (on the lower *x*-axis), and plots of the compressibility modulus (C_s^{-1})–π (on the upper *x*-axis). Peptide molar fraction: $X = 1$, $X = 0.8$, $X = 0.6$, $X = 0.4$, $X = 0.2$, $X = 0$. (B) Insightful view of a section of the plots compressibility modulus (C_s^{-1})– surface pressure (π).

(about 22 mN m^{-1}). However, π_t slightly varied when $X_{E2(347-363)}$ increased, and it disappeared for the mixture of $X_{E2(347-363)}=0.8$ (an insightful view of the transition pressure can be seen in Fig. 2B, where it is denoted by the minimum in the C_s^{-1}–π curves). From the analyses of the monolayer collapse, we can establish the hypothesis that E2(347–363) and DPPC are miscible within the whole range of surface pressure at $X_{E2(347-363)}=0.2$. However, for $X_{E2(347-363)}>0.2$ and on the basis of π_t and π_c values, we can only assume that both molecules mix at the interface for $X_{E2(347-363)}=0.8$ and at surface pressures $\leq\pi_t$.

To gain deeper insight into the behaviour of these two-dimensional systems, we have obtained and analyzed the plots of the mean molecular area (A) as a function of the film composition ($X_{E2(347-363)}$) at different surface pressures (Fig. 3). A is defined as $X_1\ A_1 + X_2\ A_2$, where A_1 and A_2 are the mean molecular areas per molecule of a pure component (1 or 2) at the particular surface pressure, and X_1 and X_2 denote the molar fraction of component 1 and 2 in the monolayer. The selected surface pressures correspond to different states of the recorded isotherms. The relationships presented in the solid lines and symbols are compared to the theoretical values (dashed lines) calculated following the additivity rule (obeyed for either immiscible or ideal mixtures of the components) [45]. Fig. 3 shows the negative deviations of the ideal behaviour for $X_{E2(347-363)}>0.2$, which increased with the amount of peptide in the monolayer. Our thermodynamic data demonstrate that both components are miscible at the interface at the surface pressures studied in this work, and their molecular interactions cause a contraction of the mixed film. This could be due to the existence of greater cohesive forces between the unlike molecules in the mixed films than between the like molecules in the pure monolayers. At the lowest peptide molar ratio ($X_{E2(347-363)}=0.2$), the components of the binary monolayer behave nearly ideally.

For a deeper thermodynamic approach to the intermolecular interactions between E2(347–363) and the lipid DPPC in the monolayer, we have calculated the excess Gibbs free energy of mixing (ΔG_M^{EX}) [46,47] defined as follows:

$$\Delta G_M^{EX} = \int_{\pi\to 0}^{\pi} A d\pi - X_1 \int_{\pi\to 0}^{\pi} A_1 d\pi - X_2 \int_{\pi\to 0}^{\pi} A_2 d\pi.$$

Numerical data were calculated from the compression isotherms according to the mathematical method of Simpson. For ideal 2D solutions, A^{EX} (excess area $=(A-(A_1X_1+A_2X_2))$ and ΔG_M^{EX} are equal to zero, but such a situation is extremely rare, and usually mixed monolayers do not behave ideally. The results exhibited negative values of ΔG_M^{EX} over the whole range of peptide concentrations, and only for $X_{E2(347-363)}=0.2$ did ΔG_M^{EX} become slightly positive at the lower surface pressure studied (Table 2). ΔG_M^{EX} has a tendency to increase with increasing surface pressure; thus, the maximum negative values were obtained at the highest pressures studied and for the $X_{E2(347-363)}=0.2$. Moreover, if the absolute values of the excess free energy are compared with RT (which amounts to 2435 J mol^{-1} where R the ideal gas constant and T the experimental temperature), it is clear that only at high surface pressures (20 and 25 mN m^{-1}) do these interactions become relevant [48]. From a biochemical point of view, this fact is of interest because this surface pressure is near to the lateral pressure found in human erythrocyte cell membranes [49].

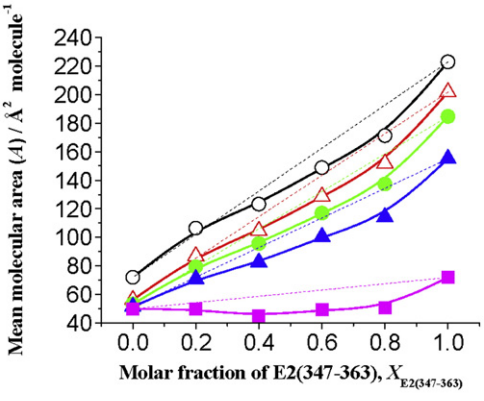

Fig. 3. Plots of mean molecular area (A) as a function of the peptide molar fractions ($X_{E2(347-363)}$) at different surface pressures (mN m^{-1}) for pure and mixed E2(347–363)/DPPC monolayers. Surface pressures: —○— 5 mN m^{-1}, —△— 10 mN m^{-1}, —●— 15 mN m^{-1}, —▲— 20 mN m^{-1}, —■— 25 mN m^{-1}.

Table 2
ΔG_M^{EX} in J mol^{-1} for different peptide–lipid mixtures at various surface pressures.

ΔG_M^{EX}/J mol^{-1}					
		$X_{E2(347-363)}$			
	π/mN m^{-1}	0.8	0.6	0.4	0.2
DPPC	5	−203.37	−254.81	−216.81	4.14
	10	−527.96	−281.03	−318.89	−74.93
	15	−1570.04	−616.15	−814.12	−651.70
	20	−4417.66	−1750.75	−2182.87	−2370.28
	25	–	–	–	−8671.59
DOPG	5	–	−246.82	−254.30	−326.87
	10	–	−311.55	−276.54	−404.65
	15	–	−511.43	−448.79	−606.20
	20	–	−1688.69	−1772.18	−1895.76
	25	–	−7240.76	−8144.92	−7941.05

Peptide and lipid solutions were dissolved in chloroform/methanol (9:1:v/v) mixture and dropped on the surface of HEPES 5 mM, NaCl 100 mM pH 7.4. The experiments were carried out at 293 K.

However, the sign and value of A^{EX} or ΔG_M^{EX} alone are not enough to determine the miscibility between the film-forming components; the analyses of A^{EX} or ΔG_M^{EX} together with the microscopic visualization of the monolayer morphology can provide the complete characteristics of the 2D system. Thus, BAM was applied for the visualization of the investigated monolayers. Representative images of the E2(347–363)/DPPC mixtures are shown in Fig. 4 (the images obtained for the $X_{E2(347-363)}=0.4$ were similar to the images obtained for $X_{E2(347-363)}=0.6$, and are thus not shown). The monolayers are homogeneous until the start of the DPPC LE–LC phase transition (for $X_{E2(347-363)}\leq 0.6$). The observed LC DPPC domains became smaller as $X_{E2(347-363)}$ increased in the film (images 4A and 4D). For the highest peptide molar ratio ($X_{E2(347-363)}=0.8$), a homogeneous monolayer was observed from the gas phase up until the beginning of the peptide collapse (image 4G). For $X_{E2(347-363)}>0.2$, brilliant dispersed nuclei can be observed at surface pressures above 20 mN m^{-1}, which are characteristics of a three-dimensional (3D) phase existing at the interface (images 4E and 4H). However, the number of these aggregates increased with $X_{E2(347-363)}$ and upon compression within the E2(347–363) collapses (images 4F and 4I). This fact demonstrates that the peptide aggregates in the presence of the lipid, and the numbers of these 3D crystals increased in the binary systems (for molar ratios higher than 0.2) with respect to the pure peptide film (Fig. 5 shows images of the pure peptide collapse). The mixed monolayer collapse could only be observed for $X_{E2(347-363)}=0.2$, where it was reflected by the appearance of linear fractures in the film.

As was previously discussed, E2(347–363) and DPPC would be miscible for $X_{E2(347-363)}=0.2$ on the basis of monolayer collapse and the DPPC transition pressure. However, the presence of the DPPC LC domains at the characteristic transition pressures, which diminished in size as the $X_{E2(347-363)}$ increased until completely disappearing at $X_{E2(347-363)}=0.8$, indicates that both components do not form a real mixture in the monolayer. Some DPPC condensed domains were soaked up in regions of the interface covered by the LE phase of the mixed monolayer, forming a *two-dimensional colloid* at the interface. This consists in a particular system (appearing in the images 4A and 4D) where the DPPC LC domains (behaving as two-dimensional micelles) are included in regions of the mixed monolayer. Thus, a

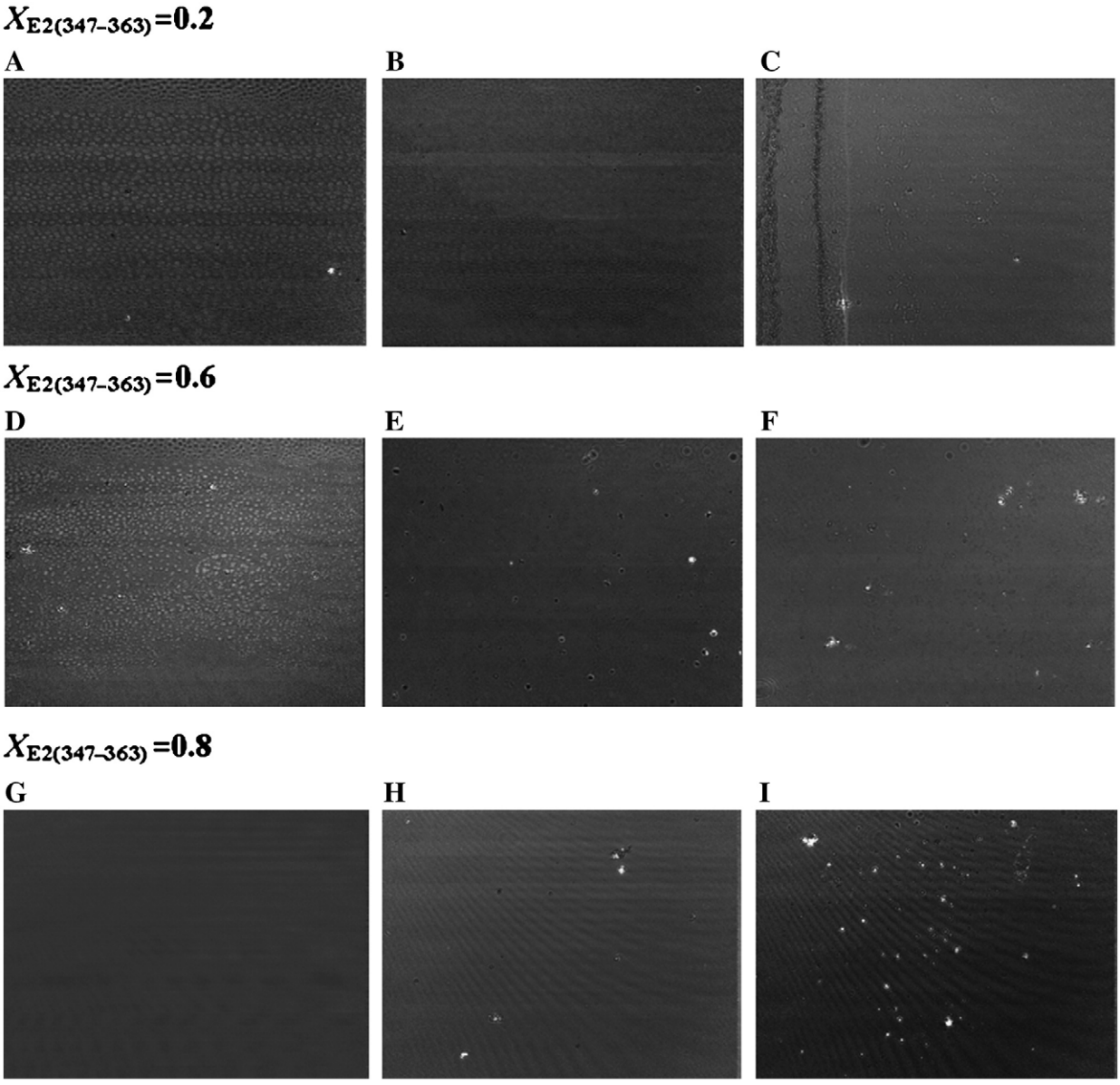

Fig. 4. BAM images corresponding to different states of the E2(347–363)/DPPC mixed monolayers spread on HEPES 5 mM, NaCl 100 mM pH 7.4. $X_{E2(347-363)}=0.2$: (A) DPPC transition, (B) start of the peptide collapse, and (C) the monolayer collapse. $X_{E2(347-363)}=0.6$: (D) DPPC transition, (E) start of the peptide collapse, and (F) end of the peptide collapse. $X_{E2(347-363)}=0.8$: (G) at 5 mN m^{-1}, (H) start of the peptide collapse, and (I) end of the peptide collapse.

partial miscibility of the two film-forming molecules takes place in the film, and the size and the environment of the DPPC LC domains change as $X_{E2(347-363)}$ increases. This fact causes: (i) the slight variation of the DPPC phase transition pressure as the amount of peptide increases in the monolayer and (ii) the decreasing of the monolayer collapse pressure at $X_{E2(347-363)}=0.2$. Moreover, the peptide starts to aggregate

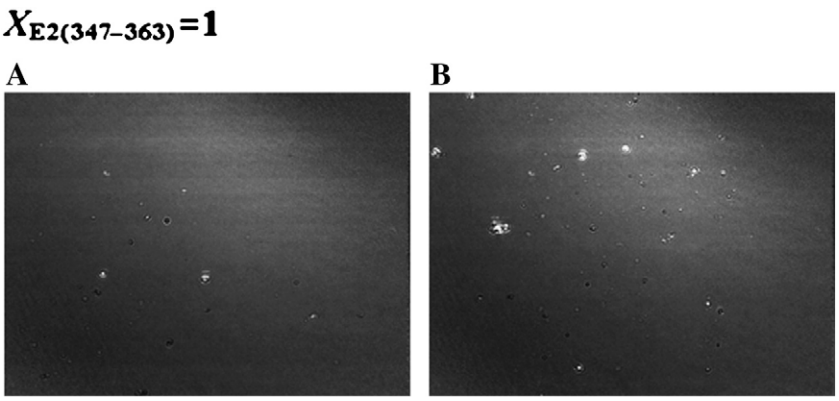

Fig. 5. BAM images corresponding to the E2(347–363) pure monolayer. (A) Start of collapse and (B) end of collapse.

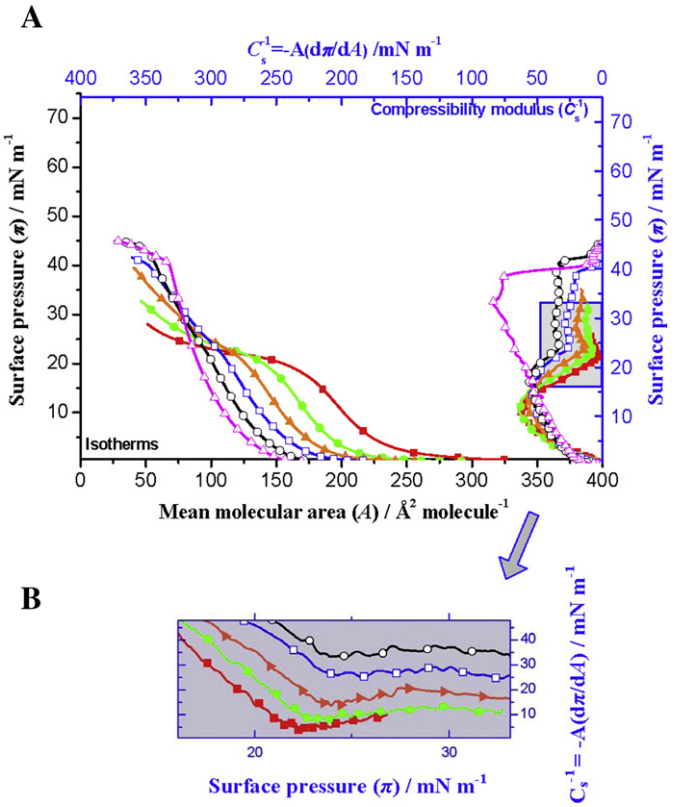

Fig. 6. (A) Surface pressure (π)–mean molecular area (A) of pure and mixed E2(347–363)/DOPG monolayers spread on subphase HEPES 5 mM, NaCl 100 mM pH 7.4 (on the lower x-axis) and plots of compressibility modulus (C_s^{-1})–π (on the upper x-axis). Peptide molar fraction: $X=1$, $X=0.8$, $X=0.6$, $X=0.4$, $X=0.2$, $X=0$. (B) Insightful view of a section of the plots compressibility modulus (C_s^{-1})– surface pressure (π).

at $\pi>20$ mN m^{-1}, which means that DPPC does not inhibit this process as was previously described in the literature for other peptides in the presence of lipid monolayers [26]; on the contrary, DPPC accelerates the ejection of E2(347–363) from the mixed films ($X_{E2(347-363)}\geq 0.4$) in order to form a 3D solid phase at surface pressures above the peptide collapse.

Thus, in monolayers of $X_{E2(347-363)}<0.8$ and at surface pressures below the peptide collapse, the DPPC and the E2(347–363) form a 2D colloidal mixture, in which the DPPC domains of condensed phase are included in regions of the interface covered with the mixed monolayer. The negative deviations from the ideality are a consequence of the existence of attractive intermolecular interactions between the peptide and the lipid in the mixed film and prove that both molecules are partially miscible at the interface at $\pi<22$ mN m^{-1} (at which point the peptide collapse starts). The peptidic sequence (17 amino acids) could adopt in the mixed monolayers (facilitated by the lateral surface pressure) a conformation which favours the hydrophobic interactions with the lipid hydrocarbon tails. Thus, the folding of the less polar peptide residues towards air would just occur at pressures below π_c and would favour the inclusion of the peptide in the monolayer (see Fig. 9A for illustration). The fact that these deviations became stronger at high surface pressures (>20 mN m^{-1}) is attributed to an acceleration of the peptide aggregation occurring at the interface, which causes a diminution of the total area occupied by the binary film with respect to the molecular areas recorded in the pure monolayers at a given surface pressure.

3.3. Mixed monolayers of E2(347–363)/DOPG

Mixed and pure isotherms of the peptide and the anionic lipid DOPG are shown in Fig. 6A. The higher fluidity of the DOPG monolayer at the experimental temperature (293 K) expanded the isotherm and resulted in a drastic diminution of the collapse pressure (~45 mN m^{-1}). As the peptide molar fraction decreased, the lift-off area of the mixed films took on values from 282.2 Å^2 molecule^{-1} for the pure peptide monolayer to 226.4, 205.6, 185.9 and 162.1 Å^2 molecule^{-1} for $X_{E2(347-363)}=0.8$, 0.6, 0.4 and 0.2, respectively. Plots of monolayer compressibility vs. surface pressure are shown in Fig. 6A. The pure DOPG monolayer reached a maximum of 80 mN m^{-1}, and the peptide and its mixtures ranged between 40 and 60 mN m^{-1}, values which are characteristic of a LE state. The monolayer collapse pressure could only be determined for the mixture of $X_{E2(347-363)}=0.2$, and its value is similar to that obtained for the pure DOPG monolayer. On the other hand, π_c increased with the lipid molar ratio from 22 mN m^{-1} to near 26 mN m^{-1} (Fig. 6B).

Plots of the mean molecular area vs. the peptide molar fraction (Fig. 7) show slight negative deviations from ideality at surface pressures of 5, 10 and 15 mN m^{-1}, which decreased as the surface pressure increased until behaving nearly linear at 20 mN m^{-1}. Nevertheless, at 25 mN m^{-1}, a surprisingly high positive deviations was observed, with a maximum for $X_{E2(347-363)}=0.6$. The ΔG_M^{EX} values, shown in Table 2, are lower than those corresponding to the peptide/DPPC mixtures and are consistent with the existence of weak intermolecular interactions between the film-forming molecules at the interface.

BAM images (Fig. 8) show homogeneous films (image 8A) for $X_{E2(347-363)}<0.8$ within the whole compression (results not shown for the $X_{E2(347-363)}=0.4$ and 0.6). Some isolated brilliant nuclei have been observed only after reaching the monolayer collapse at $X_{E2(347-363)}=0.2$ (image 8B). For the $X_{E2(347-363)}=0.8$ disperse 3D aggregates appeared at the interface during the gas phase; the number and size of these crystals did not increase until reaching pressures above the *plateau* characteristic of the peptide collapse.

The above results may be interpreted as follows. For $X_{E2(347-363)}<0.8$ and at surface pressures below π_c of the mixed films, both molecules are miscible, with the existence of weak electrostatic attractive forces between the peptide (positively charged) and the anionic lipid at the interface, which causes the negative deviations from the ideality. In this case, the peptide would adopt a conformation at the interface that favours the attractive interactions between its positive charge groups and the DOPG polar head. These interactions anchor the peptide to the lipid polar head, which is partially immersed in the subphase, and stabilize the peptide at the interface (see Fig. 9B). As a result, the value of surface pressure at which the peptide collapse starts in the mixed films (Fig. 6B) increases and, at surface pressures above π_c, the aggregation is inhibited in the presence of DOPG. The absence of 3D crystal formation at high surface pressures results in an increase of the mean molecular

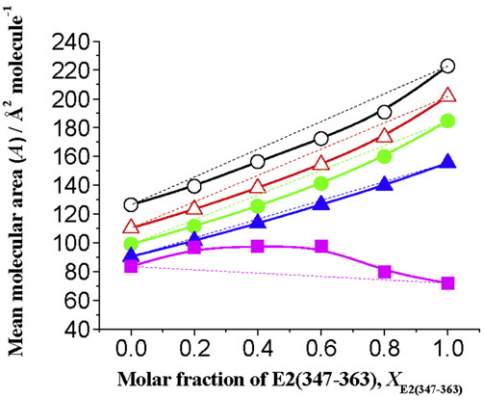

Fig. 7. Plots of mean molecular area (A) as a function of the peptide molar fractions ($X_{E2(347-363)}$) at different surface pressures (mN m^{-1}) for pure and mixed E2(347–363)/DOPG monolayers. Surface pressures: 5 mN m^{-1}, 10 mN m^{-1}, 15 mN m^{-1}, 20 mN m^{-1}, 25 mN m^{-1}.

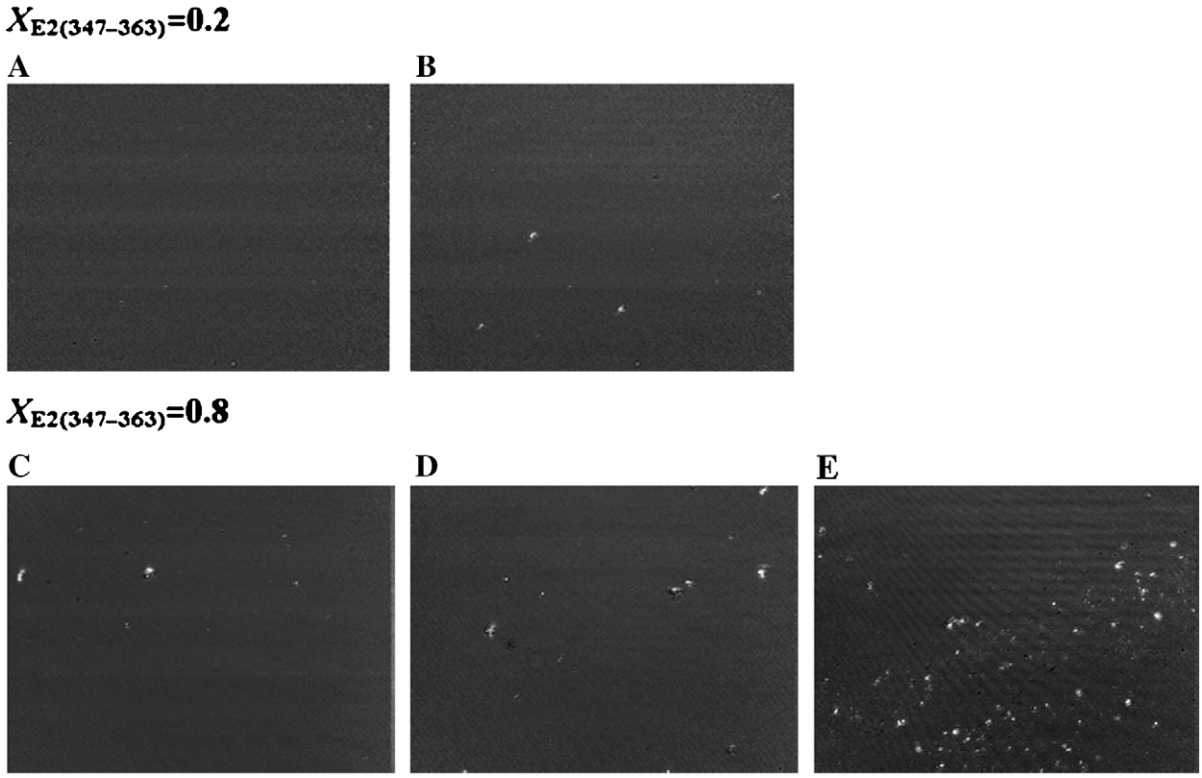

Fig. 8. BAM images corresponding to different states of compression for E2(347–363)/DOPG mixed monolayers spread on HEPES 5 mM, NaCl 100 mM pH 7.4. $X_{E2(347-363)} = 0.2$: (A) gas phase; (B) monolayer collapse. $X_{E2(347-363)} = 0.8$: (C) gas phase; (D) start of the peptide collapse; and (E) end of the peptide collapse.

area in the mixed monolayer with respect to the pure peptide film and causes the positive deviations from ideality observed at high surface pressures for $X_{E2(347-363)} < 0.8$. For the $X_{E2(347-363)} = 0.8$ the peptide is partially squeezed out from the gaseous monolayer to form disperse 3D aggregates, which diminishes the positive deviation observed for the highest peptide molar ratio.

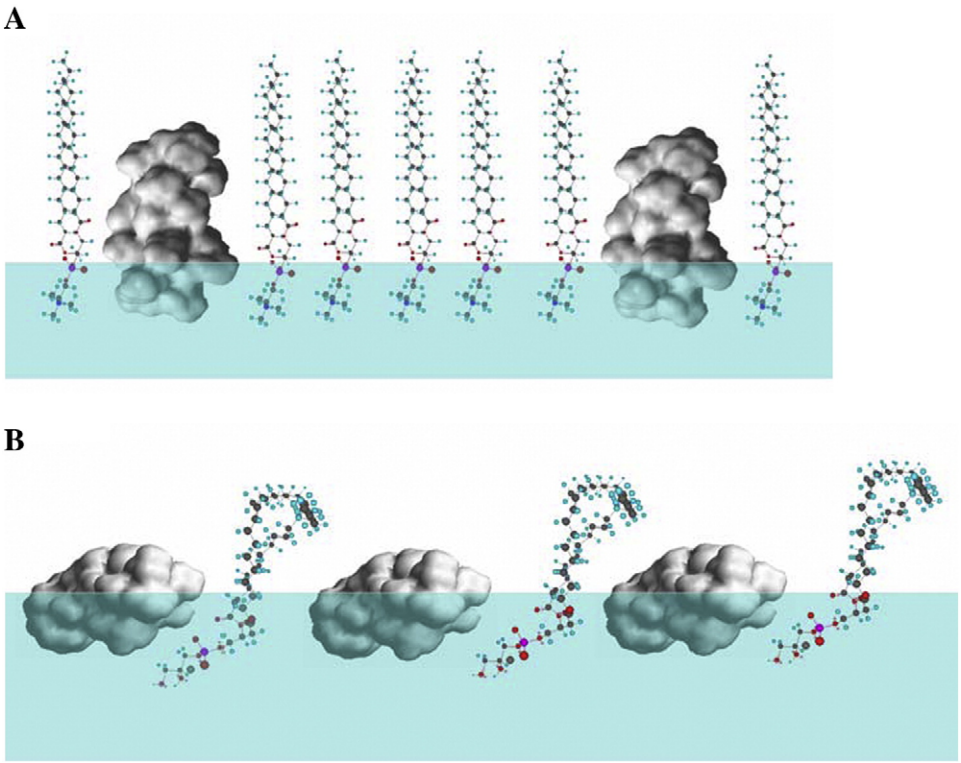

Fig. 9. Illustrative schemes showing the peptide/lipid mixed monolayers. (A) Peptide/DPPC monolayers for $X_{E2(347-363)} < 0.8$ at surface pressures below the peptide collapse (5–22 mN m^{-1}); and (B) peptide/DOPG monolayer for $X_{E2(347-363)} < 0.8$ at about 24–26 mN m^{-1}.

4. Conclusions

We have studied the behaviour of Langmuir monolayers of a synthetic peptide named E2(347–363), from the GB virus C/Hepatitis G virus, in the presence of DPPC and DOPG. The results have proven that the peptide forms a stable monolayer, which adopts a well-extended configuration at the air–water interface. The peptide and DPPC are partially miscible and form a two-dimensional colloidal mixture for $X_{E2(347-363)}<0.8$ and at surface pressures above the DPPC lipid transition and below the peptide collapse. The attractive interactions between the film-forming molecules become stronger upon film compression, being relevant at $\pi=20$ mN m^{-1}. At $\pi>20$ mN m^{-1} the peptide is ejected from the mixed film in order to form a three-dimensional solid phase. This aggregation process is slightly accelerated by the lipid in the DPPC/peptide mixed monolayers only when $X_{E2(347-363)}>0.2$.

On the other hand, weak electrostatic attractive forces between the peptide (positively charged) and the anionic lipid (DOPG) (i) cause negative deviations from the ideality, (ii) stabilize the peptide at the interface and (iii) increase the value of surface pressure at which the peptide collapses. The anionic lipid inhibits the peptide aggregation in the monolayer for $X_{E2(347-363)}<0.8$. This causes the positive deviations from ideality observed at high surface pressures. For the $X_{E2(347-363)}=0.8$, the peptide forms disperse three-dimensional aggregates within the gas state of the monolayer.

In conclusion, the peptide E2(347–363) interacts with the two membrane models (DPPC and DOPG Langmuir monolayers) studied in this paper, and the behaviour of the peptide at the interface, as well as the forces between the film-forming molecules, depends on the monolayer composition, on the surface pressure and on the nature of the lipid. Therefore, we argue in favour of considering the E2(347–363) peptide sequence a good candidate for developing further experiments in order to determine its potential role in the fusion mechanism that regulates the entry of the GBV-C/HGV virus into cells.

Acknowledgements

This work was supported by grants from the Ministerio de Ciencia e Innovación (Secretaría de Estado de Universidades, Dirección General de Programas y Transferencia de Conocimiento, Subdirección General de Proyectos de Investigación, Spain) CTQ 2006-15396-C02-01, CTQ 2006-15396-C02-02 and CTQ 2006-04085/BQU, and N. Vila-Romeu would also like to thank Xunta de Galicia for the grant of Rf. PGDIT06PXIB383004PR. The authors thank Rafael Zabala de Oleza for taking part in the synthesis of the studied peptide.

References

[1] J. Linnen, J. Wages Jr., Z.Y. Zhang-Keck, K.E. Fry, K.Z. Krawczynski, H. Alter, E. Koonin, M. Gallagher, M. Alter, S. Hadziyannis, P. Karayiannis, K. Fung, Y. Nakatsuji, J.W. Shih, L. Young, M. Piatak Jr., C. Hoover, J. Fernandez, S. Chen, J.C. Zou, T. Morris, K.C. Hyams, S. Ismay, J.D. Lifson, G. Hess, S.K. Foung, H. Thomas, D. Bradley, H. Margolis, J.P. Kim, Molecular cloning and disease association of hepatitis G virus: a transfusion-transmissible agent, Science 271 (1996) 505–508.
[2] J.N. Simons, T.P. Leary, G.J. Dawson, T.J. Pilot-Matias, A.S. Muerhoff, G.G. Schlauder, S.M. Desai, I.K. Mushahwar, Isolation of novel virus-like sequences associated with human hepatitis, Nat. Med. 1 (1995) 564–569.
[3] L.D. Moaven, I.F. Young, D.S. Bowden, S.A. Locarnini, Prevalence of hepatitis G virus antibodies in Queensland blood donors, Med. J. Aust. 166 (1997) 507–509.
[4] H.J. Alter, G-pers creepers, where'd you get those papers? A reassessment of the literature on the hepatitis G virus, Transfusion 37 (1997) 569–572.
[5] J.T. Stapleton, GB virus type C/hepatitis G virus, Semin. Liver. Dis. 23 (2003) 137–148.
[6] P. Abraham, GB virus C/hepatitis G virus—its role in human disease redefined? Indian J. Med. Res. 125 (2007) 717–719.
[7] P.M. Polgreen, J. Xiang, Q. Chang, J.T. Stapleton, GB virus type C/hepatitis G virus: a non-pathogenic flavivirus associated with prolonged survival in HIV-infected individuals, Microbes Infect. 5 (2003) 1255–1261.
[8] J. Takamatsu, H. Toyoda, Y. Fukuda, GB virus C and mortality from HIV infection, N. Engl. J. Med. 346 (2002) 377–379.
[9] D.T. Lau, K.D. Miller, J. Detmer, J. Kolberg, B. Herpin, J.A. Metcalf, R.T. Davey, J.H. Hoofnagle, Hepatitis G virus and human immunodeficiency virus coinfection: response to interferon-alpha therapy, J. Infect. Dis. 180 (1999) 1334–1337.
[10] F. Puig-Basagoiti, M. Cabana, M. Guilera, M. Gimenez-Barcons, G. Sirera, C. Tural, B. Clotet, J.M. Sanchez-Tapias, J. Rodes, J.C. Saiz, M.A. Martinez, Prevalence and route of transmission of infection with a novel DNA virus (TTV), hepatitis C virus, and hepatitis G virus in patients infected with HIV, J. Acquir. Immune Defic. Syndr. 23 (2000) 89–94.
[11] H.L. Tillmann, M.P. Manns, GB virus-C infection in patients infected with the human immunodeficiency virus, Antiviral Res. 52 (2001) 83–90.
[12] T. Cohen, M. Pevsner-Fischer, N. Cohen, I.R. Cohen, Y. Shai, Characterization of the interacting domain of the HIV-1 fusion peptide with the transmembrane domain of the T-cell receptor, Biochemistry 47 (2008) 4826–4833.
[13] M.R. Moreno, J. Guillen, A.J. Perez-Berna, D. Amoros, A.I. Gomez, A. Bernabeu, J. Villalain, Characterization of the interaction of two peptides from the N terminus of the NHR domain of HIV-1 gp41 with phospholipid membranes, Biochemistry 46 (2007) 10,572–10,584.
[14] W. Weissenhorn, A. Hinz, Y. Gaudin, Virus membrane fusion, FEBS Lett. 581 (2007) 2150–2155.
[15] J.M. White, Viral and cellular membrane fusion proteins, Annu. Rev. Physiol. 52 (1990) 675–697.
[16] R.M. Epand, Fusion peptides and the mechanism of viral fusion, BBA-Biomembranes 1614 (2003) 116–121.
[17] R. Jahn, T.C. Sudhof, Membrane fusion and exocytosis, Annu. Rev. Biochem. 68 (1999) 863–911.
[18] S. Jung, M. Eichenmuller, N. Donhauser, F. Neipel, A.M. Engel, G. Hess, B. Fleckenstein, H. Reil, HIV entry inhibition by the envelope 2 glycoprotein of GB virus C, AIDS 21 (2007) 645–647.
[19] J.P. Kim, K.E. Fry, Molecular characterization of the hepatitis G virus, J. Viral Hepat. 4 (1997) 77–79.
[20] A.T. Yagnik, A. Lahm, A. Meola, R.M. Roccasecca, B.B. Ercole, A. Nicosia, A. Tramontano, A model for the hepatitis C virus envelope glycoprotein E2, Proteins 40 (2000) 355–366.
[21] J. Lescar, A. Roussel, M.W. Wien, J. Navaza, S.D. Fuller, G. Wengler, G. Wengler, F.A. Rey, The fusion glycoprotein shell of Semliki Forest virus: an icosahedral assembly primed for fusogenic activation at endosomal pH, Cell 105 (2001) 137–148.
[22] J. Guillen, M.R. Moreno, A.J. Perez-Berna, A. Bernabeu, J. Villalain, Interaction of a peptide from the pre-transmembrane domain of the severe acute respiratory syndrome coronavirus spike protein with phospholipid membranes, J. Phys. Chem. B 111 (2007) 13,714–13,725.
[23] G.L. Gaines, Insoluble Monolayers at Liquid–Gas Interfaces, Interscience, New York, 1966.
[24] D.H. Lopes, A. Meister, A. Gohlke, A. Hauser, A. Blume, R. Winter, Mechanism of islet amyloid polypeptide fibrillation at lipid interfaces studied by infrared reflection absorption spectroscopy, Biophys. J. 93 (2007) 3132–3141.
[25] M. Meier, X.L. Blatter, A. Seelig, J. Seelig, Interaction of verapamil with lipid membranes and P-glycoprotein: connecting thermodynamics and membrane structure with functional activity, Biophys. J. 91 (2006) 2943–2955.
[26] S. Pérez-López, N. Vila-Romeu, M.A. Alsina Esteller, M. Espina, I. Haro, C. Mestres, Interaction of GB virus C/hepatitis G virus synthetic peptides with lipid Langmuir monolayers and large unilamellar vesicles, J. Phys. Chem. B 113 (2009) 319–327.
[27] K. Boesze-Battaglia, R. Schimmel, Cell membrane lipid composition and distribution: implications for cell function and lessons learned from photoreceptors and platelets, J. Exp. Biol. 200 (1997) 2927–2936.
[28] G. Van Meer, I.L. Van Genderen, in: H.J. Hilderson, G.B. Ralston (Eds.), Intracellular Lipid Distribution, Transport and Sorting: A Cellbiologist's Need for Physicochemical Information, Subcellular Biochemistry: Physicochemical Methods in the Study of Biomembranes, Plenum Press, New York, 1995, pp. 1–120.
[29] M. Nieto-Suárez, N. Vila-Romeu, P. Dynarowicz-Latka, Behavior of insulin–sphingomyelin mixed Langmuir monolayers spread at the air–water interface, Colloids Surfaces A: Physicochem. Eng. Aspects 321 (2008) 189–195.
[30] S. Pérez, J. Miñones, M. Espina, M.A. Alsina, I. Haro, C. Mestres, Influence of the saturation chain and head group charge of phospholipids in the interaction of hepatitis G virus synthetic peptides, J. Phys. Chem. B 109 (2005) 19,970–19,979.
[31] M.A. Larkin, G. Blackshields, N.P. Brown, R. Chenna, P.A. McGettigan, H. McWilliam, F. Valentin, I.M. Wallace, A. Wilm, R. Lopez, J.D. Thompson, T.J. Gibson, D.G. Higgins, Clustal W and Clustal X version 2.0, Bioinformatics 23 (2007) 2947–2948.
[32] T.P. Hopp, K.R. Woods, Prediction of protein antigenic determinants from amino acid sequences, Proc. Natl. Acad. Sci. U.S.A. 78 (1981) 3824–3828.
[33] J. Janin, Surface and inside volumes in globular proteins, Nature 277 (1979) 491–492.
[34] G.W. Welling, W.J. Weijer, Z.R. van der, S. Welling-Wester, Prediction of sequential antigenic regions in proteins, FEBS Lett. 188 (1985) 215–218.
[35] P.Y. Chou, G.D. Fasman, Prediction of the secondary structure of proteins from their amino acid sequence, Adv. Enzymol. Relat Areas Mol. Biol. 47 (1978) 45–148.
[36] T.S. Jardetzky, R.A. Lamb, Virology: a class act, Nature 427 (2004) 307–308.
[37] M. Nieto-Suárez, N. Vila-Romeu, I. Prieto, Behaviour of insulin Langmuir monolayers at the air–water interface under various conditions, Thin Solid Films 516 (2008) 8873–8879.
[38] D.J. Crisp, A Two Dimensional Phase Rule. I. Derivatization of a Two-Dimensional Phase Rule for Plane Interfaces, Surface Chemistry, Butterworths, London, 1949.
[39] C.W.N. Cumper, A.E. Alexander, The surface chemistry of proteins, Trans. Faraday Soc. 46 (1950) 235–253.
[40] N. Vila Romeu, J. Miñones Trillo, O. Conde, M. Casas, E. Iribarnegaray, Influence of several factors on the response of calcitonin monolayers to compression at the air–water interface, Langmuir 13 (1997) 71–75.

[41] S. Steinkopf, A.K. Schelderup, H.L. Gjerde, J. Pfeiffer, S.v. Thoresen, A.U. Gjerde, H. Holmsen, The psychotropic drug olanzapine (Zyprexa) increases the area of acid glycerophospholipid monolayers, Biophys. Chem. 134 (2008) 39–46.
[42] G.L. Gaines, in: I. Prigogine (Ed.), Properties of Liquid Surface, Insoluble Monolayers at Liquid–Gas Interfaces, Interscience, New York, 1966, p. 24.
[43] J.T. Davies, R.K. Rideal, Interfacial Phenomena, Academic Press, New York, 1963, p. 265, 2ª Edition.
[44] P. Dynarowicz-Latka, K. Kita, Molecular interaction in mixed monolayers at the air/water interface, Adv. Colloid Interface Sci. 79 (1999) 1–17.
[45] J.B. Li, J. Krägel, A.V. Makievski, V.B. Fainermann, R. Miller, H. Möhwald, A study of mixed phospholipid/[beta]-casein monolayers at the water/air surface, Colloids Surfaces A: Physicochem. Eng. Aspects 142 (1998) 355–360.
[46] F.C. Goodrich, Proceedings of the 11th International Congress on Surface Activity, , 1957.
[47] R.E. Pagano, N.L. Gershfeld, A millidyne film balance for measuring intermolecular energies in lipid films, J. Colloid Interface Sci. 41 (1972) 311–317.
[48] M.A. Alsina, C. Mestres, G. Valencia, J.M.G. Antón, F. Reig, Interaction energies of mixing phosphatidylserine and phosphatidylcholine monolayers, Colloids Surfaces 34 (1988) 151–158.
[49] R.F.A. Zwaal, R.A. Demel, B. Roelofsen, L.L.M. van Deenen, The lipid bilayer concept of cell membranes, Trends Biochem. Sci. 1 (1976) 112–114.